PHYSICAL REVIEW E **94**, 061101(R) (2016)

Statistical theory of reversals in two-dimensional confined turbulent flows

Vishwanath Shukla,* Stephan Fauve,† and Marc Brachet‡
Laboratoire de Physique Statistique, École Normale Supérieure, PSL Research University; UPMC Univ Paris 06, Sorbonne Universités; Université Paris Diderot, Sorbonne Paris-Cité; and CNRS, 24 Rue Lhomond, 75005 Paris, France
(Received 26 June 2016; published 1 December 2016)

It is shown that the truncated Euler equation (TEE), i.e., a finite set of ordinary differential equations for the amplitude of the large-scale modes, can correctly describe the complex transitional dynamics that occur within the turbulent regime of a confined two-dimensional flow obeying Navier-Stokes equation (NSE) with bottom friction and a spatially periodic forcing. The random reversals of the NSE large-scale circulation on the turbulent background involve bifurcations of the probability distribution function of the large-scale circulation. We demonstrate that these NSE bifurcations are described by the related TEE microcanonical distribution which displays transitions from Gaussian to bimodal and broken ergodicity. A minimal 13-mode model reproduces these results.

DOI: 10.1103/PhysRevE.94.061101

The formation of large-scale coherent structures is widely observed in atmospheric and oceanic flows and ascribed to the nearly bidimensional nature of these flows. Kraichnan showed that in two-dimensional (2D) turbulence, the energy is transferred from the forcing scale to larger scales due to the conservation of both energy and enstrophy by the inviscid dynamics [1]. In a confined flow domain and without large-scale friction, the energy accumulates at the largest possible scale, thus generating coherent structures in the form of large-scale vortices.

It has been observed in laboratory experiments that the large-scale circulation generated by forcing a nearly 2D flow at small scale can display random reversals [2]. The large-scale velocity has a bimodal probability density function (PDF) with two symmetric maxima related to the opposite signs of the large-scale circulation. This regime bifurcates from another turbulent regime with a Gaussian velocity field with zero mean when the large-scale friction is decreased. When the friction is decreased further, the reversals become less and less frequent and a condensed state with most of its kinetic energy in the large-scale circulation is reached [3]. A similar sequence of transitions is observed in numerical simulations of the 2D Navier-Stokes equation (NSE) with large-scale friction and spatially periodic forcing [4].

These transitions correspond to bifurcations of a mean flow on a strongly turbulent background for which no theoretical tool exists so far. We show in this Rapid Communication that the truncated Euler equation (TEE), i.e., a finite set of ordinary differential equations (ODEs) for the amplitude of the large-scale modes without forcing and dissipation, can correctly describe these transitions. To wit, we compare the dynamical regimes observed in numerical simulations of the 2D NSE with the ones obtained with the TEE when the characteristic scale k_c^{-1} of the initial conditions is changed, with $k_c = \sqrt{\Omega/E}$ where E is the kinetic energy of the flow and Ω is its enstrophy (integrated squared vorticity).

The dimensionless 2D NSE reads for an incompressible velocity field $\mathbf{u} = \boldsymbol{\nabla} \times (\psi \hat{\mathbf{z}})$,

$$\frac{\partial \psi}{\partial t} - \frac{1}{\nabla^2}\{\psi, \nabla^2 \psi\} = -\frac{1}{\mathrm{Rh}}\psi + \frac{1}{\mathrm{Re}}\nabla^2 \psi + f_\psi, \qquad (1)$$

where $\psi(x,y,t)$ is the stream function and $\{f,g\} = \partial_x f \partial_y g - \partial_x g \partial_y f$ is the usual Poisson bracket. The first term on the right-hand side represents the frictional force in the bottom boundary layer and $\boldsymbol{\nabla} \times (f_\psi \hat{\mathbf{z}})$ is the spatially periodic forcing, explicitly given by $f_\psi = \frac{1}{144}\sin(6x)\sin(6y)$.

To model flow confinement we use free-slip boundary conditions; therefore, the stream function can be Fourier expanded as

$$\psi(x,y) = \sum_{m,n} \hat{\psi}_{m,n} \sin(mx)\sin(ny), \qquad (2)$$

for x and y in the $[0,\pi]$ domain. The nondimensional parameters are the Reynolds number, $\mathrm{Re} = UL/\nu$ and $\mathrm{Rh} = \tau U/L$, which represents the ratio of the inertial term to the friction on the bottom boundary. Here, U is a characteristic large-scale velocity, L is the length of the square container, ν is the kinematic viscosity, and $1/\tau$ is the damping rate related to the friction. The above equation has been made dimensionless using the length scale L and the velocity scale U.

We perform direct numerical simulations (DNSs) of Eq. (1), using standard pseudospectral methods [5] with N_c^2 collocation points and 2/3 circular dealiasing: $k_{\max} = N_c/3$. Time stepping is performed with a second-order, exponential time differencing Runge-Kutta method [6]. DNSs of the NSE (1) are carried out for $\mathrm{Re} = 3000/\pi^2$ and $\mathrm{Re} = 5000/\pi^2$ with $N_c = 256$. Very long time integration is needed to accumulate reliable statistics for the reversals, which become rare with an increase in Rh (see below).

Direct time recordings of the amplitude of the lowest wave number mode of the stream function, $\hat{\psi}_{1,1}$, are displayed in Fig. 1(a) for $\mathrm{Re} = 5000/\pi^2$ and different values of Rh [7]. For $\mathrm{Rh} = 10$, the amplitude of the large-scale circulation fluctuates around zero and its PDF is Gaussian (not shown). When Rh is increased, a first transition is observed within the turbulent

*research.vishwanath@gmail.com
†fauve@lps.ens.fr
‡brachet@physique.ens.fr

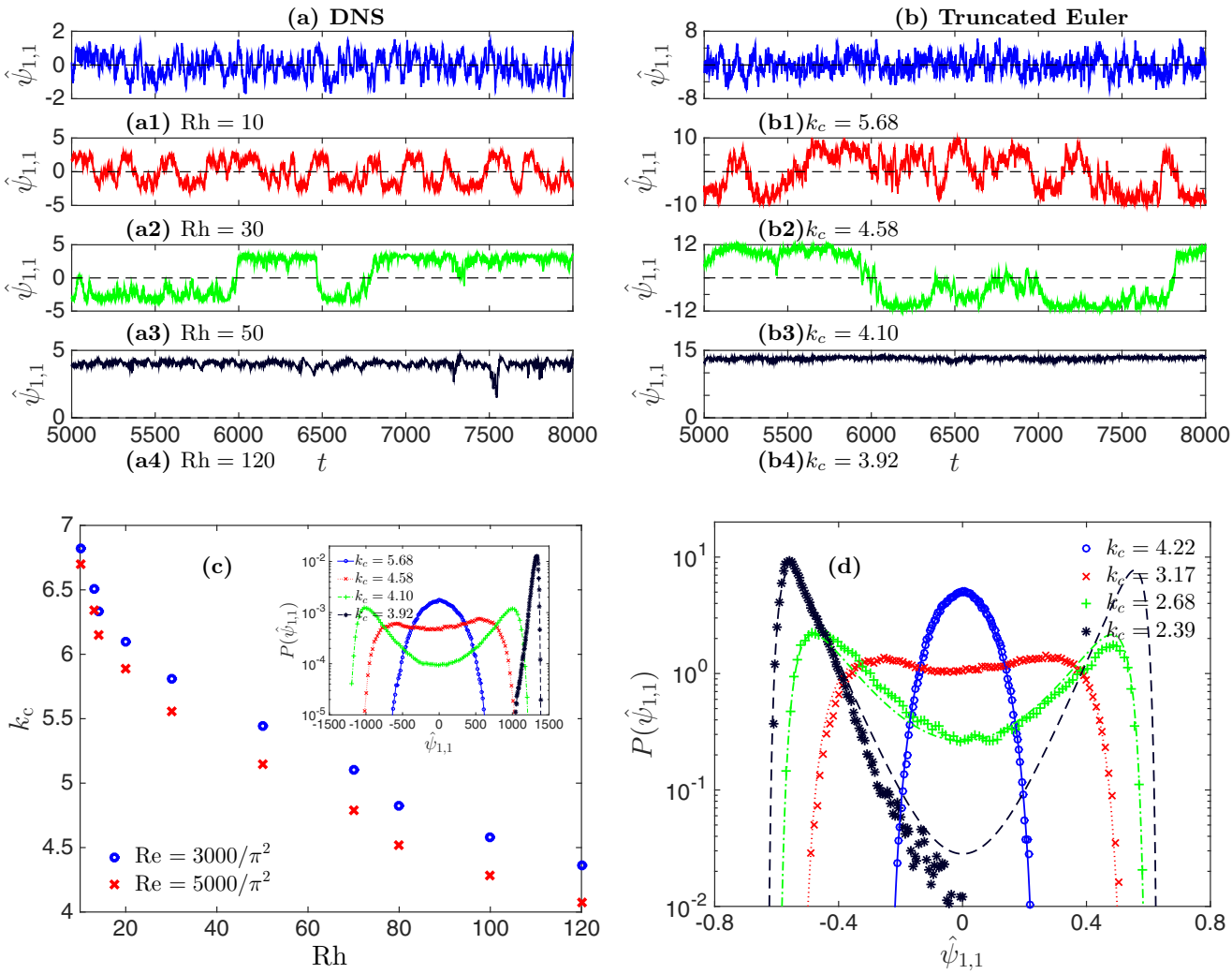

FIG. 1. Flow transitions: Time series of $\hat{\psi}_{1,1}$ obtained from the DNS of the (a) Navier-Stokes equation (NSE) for different values of Rh and Re $= 5000/\pi^2$, and (b) truncated Euler equation (TEE) for different values of k_c. $\hat{\psi}_{1,1}^{\mathrm{NSE}}$ and $\hat{\psi}_{1,1}^{\mathrm{TEE}}$ have been divided by 10^4 and 10^2, respectively. (c) Plot of $k_c = \sqrt{\Omega/E}$ versus Rh from the DNS of the NSE for two different Reynold's numbers Re $= 3000/\pi^2$ (blue circles) and Re $= 5000/\pi^2$ (red crosses). Inset: Log-linear plots of the PDFs of $\hat{\psi}_{1,1}^{TEE}$ for different values of k_c. (d) Log-linear plots of the PDFs of $\hat{\psi}_{1,1}$ for different values of k_c obtained from the finite-mode minimal model based on the TEE; the lines on top of these PDFs indicate the estimation from our analytical method.

regime and can be characterized by a change of the shape of the PDF that becomes bimodal. $\hat{\psi}_{1,1}$ fluctuates around two nonzero most probable opposite values and displays random transitions between these two states [see Fig. 1(a2)]. This corresponds to random reversals of the large-scale circulation on a turbulent background. The mean waiting time between successive reversals increases with Rh [see Fig. 1(a3)] and finally a large-scale circulation with a given sign becomes the dominant flow component [see Fig. 1(a4)]. This is the condensed state described by Kraichnan [1,8]. The regime with random reversals of the large-scale circulation is therefore located in parameter space between the condensed states and the turbulent regime with Gaussian velocity PDFs as observed in experiments [3].

We now consider the approach introduced by Lee [9] and developed by Kraichnan [1,8] that relies on the 2D TEE. They showed that the Euler equation, truncated between a minimum and a maximum wave number, gives a set of ODEs for the amplitudes of the modes that follow a Liouville theorem [9]. For 2D flows, the kinetic energy E and the enstrophy Ω (integrated squared vorticity) are conserved; therefore, the Boltzmann-Gibbs canonical equilibrium distribution is of the form $\mathcal{P} = Z^{-1}\exp(-\alpha E - \beta\Omega)$, where Z is the partition function and α and β can be seen as inverse temperatures, determined by the total energy and enstrophy. Using this formalism, Kraichnan [1,8] derived the absolute equilibria of the energy spectrum $E(k)$ and showed the existence of different regimes depending on the values of α and β. On the other hand, microcanonical distributions are defined by $\delta(E - E_0)\delta(\Omega - \Omega_0)$, where E_0 and Ω_0 are respectively the energy and enstrophy of the initial conditions, and should be used to compute the PDFs in the reversal and condensed state (see below).

The TEE is obtained by performing a circular Galerkin truncation at wave number $k_{\max}$ of the incompressible, Euler equation $\frac{\partial\psi}{\partial t} - \frac{1}{\nabla^2}\{\psi, \nabla^2\psi\} = 0$, which is Eq. (1) without

forcing or dissipation. The TEE in spectral space reads

$$\frac{\partial \hat{\psi}_{\mathbf{k}}}{\partial t} = \frac{1}{k^2} \sum_{\mathbf{p},\mathbf{q}} (\mathbf{p} \times \mathbf{q}) q^2 \hat{\psi}_{\mathbf{p}} \hat{\psi}_{\mathbf{q}} \delta_{\mathbf{k},\mathbf{p}+\mathbf{q}} \tag{3}$$

with $\delta_{\mathbf{k},\mathbf{r}}$ the Kronecker delta and with Fourier modes satisfying $\hat{\psi}_{\mathbf{k}} = 0$ if $|\mathbf{k}| \geqslant k_{\max}$. Note that, because of the free-slip boundary conditions, Eq. (2), the Fourier modes $\hat{\psi}_{\mathbf{k}}$ are real numbers. This truncated system exactly conserves the quadratic invariants, energy and enstrophy, given in Fourier space by $E = \frac{1}{2}\sum_{\mathbf{k}} |\mathbf{u}_{\mathbf{k}}|^2$ and $\Omega = \frac{1}{2}\sum_{\mathbf{k}} k^2 |\mathbf{u}_{\mathbf{k}}|^2$ [10].

For TEE we take $k_{\max}$ as a free parameter and the same stream function expansion as that used for the NSE (2), thus the numerical integration method is the same as the one described above for the NSE. In both cases, the minimum wave number is $k_{\min} = \sqrt{2}$. We use an initial velocity field with an energy spectra $E(k) = k/(\alpha + \beta k^2)$, where by varying α and β we can obtain different flow regimes in accordance with Kraichnan's absolute equilibrium predictions. We introduce a wave number k_c given by $k_c^2 = \Omega/E$, which acts as an important control parameter of the system.

We next consider the results obtained using the TEE (3) with $k_{\max} = k_f$ (the NSE forcing wave number) and initial conditions with different values of k_c. Figure 1(b) shows the transitions between different turbulent regimes when k_c is decreased. The corresponding PDFs of $\hat{\psi}_{1,1}$ obtained for different values of k_c are displayed in the inset of Fig. 1(c). We observe the transition from Gaussian to bimodal PDF when k_c is decreased and then the transition to the condensed regime with a given sign of the large-scale circulation.

For NSE at large Re, the effect of the large-scale friction is to stop the inverse cascade before reaching the scale of the flow domain. Rh thus determines the largest scale of the flow and its associated wave number $k_c = (\Omega/E)^{1/2}$. Increasing Rh (decreasing bottom friction) should thus increase the largest flow scale and decrease k_c. Figure 1(c) indeed shows that k_c monotonously decreases when Rh is increased and weakly depends on Re. When Rh is large (small friction), the kinetic energy accumulates at the scale of the flow domain and the condensed state is obtained.

Although we do not have a quantitative agreement between the transition values of k_c for the TEE and NSE [see Fig. 1(c)], the same sequence of transitions is observed in both cases. Figure 1(d) shows that this qualitative agreement is maintained even for a truncation wave number as low as $k_{\max} = 2\sqrt{5}$. This truncation leads to only 13 ODEs for the amplitudes of the large-scale modes (see the Appendix). We emphasize that this minimal set of ODEs provides a noteworthy qualitative description of the transitions between the different turbulent regimes observed in DNSs and experiments.

The TEE model (3) is a finite number of quadratic nonlinear ODEs for real variables y_i [see the remark following Eq. (3) about the amplitudes of the Fourier modes noted y_i hereafter to simplify the notations] that conserve both the energy $E(t) = \sum_{j=0}^{n} b_E(j) y_j^2$ and the enstrophy $\Omega(t) = \sum_{j=0}^{n} b_\Omega(j) y_j^2$ (see the Appendix). By making use of the identities

$$(2\pi)^2 \delta(b_E y^2 - E)\delta(b_\Omega y^2 - \Omega) = \int_{-\infty}^{\infty} dp_E dp_\Omega e^{ip_E(b_E y^2 - E) + ip_\Omega(b_\Omega y^2 - \Omega)} \tag{4}$$

and

$$\int_{-\infty}^{\infty} e^{i(p_E b_E + p_\Omega b_\Omega) y^2} dy = \frac{\sqrt{\pi}}{\sqrt{-i(b_E p_E + b_\Omega p_\Omega)}} \tag{5}$$

we can write the total microcanonical phase space volume

$$\mathcal{V} = \int \prod_{j=0}^{n} dy_j \delta\left(\sum_{j=0}^{n} b_E(j) y_j^2 - E\right) \delta\left(\sum_{j=0}^{n} b_\Omega(j) y_j^2 - \Omega\right) \tag{6}$$

as

$$\mathcal{V} = \int_{-\infty}^{\infty} dp_E dp_\Omega e^{L_\mathcal{V}(p_E, p_\Omega)} \tag{7}$$

with

$$L_\mathcal{V} = \sum_{j=0}^{n} \log\left(\frac{\sqrt{\pi}}{\sqrt{-i[p_E b_E(j) + p_\Omega b_\Omega(j)]}}\right) + ip_E(-E) + ip_\Omega(-\Omega) - 2\log(2\pi). \tag{8}$$

We now apply the steepest descent method [11,12] to the integral in Eq. (7). This procedure yields

$$\mathcal{V}(p_E, p_\Omega) = 2\pi e^{L_\mathcal{V}} \left[\det(\partial^2 L_\mathcal{V}/\partial_{p_E}\partial_{p_\Omega})\right]^{-1/2}, \tag{9}$$

which furnishes an explicit parametric expression for $\mathcal{V}$ at the saddle point (p_E, p_Ω) [13] corresponding to $k_c = \sqrt{\Omega/E}$, with the values of energy and enstrophy given by the saddle conditions

$$E(p_E, p_\Omega) = i \sum_{j=0}^{n} \frac{b_E(j)}{2[p_E b_E(j) + p_\Omega b_\Omega(j)]},$$
$$\Omega(p_E, p_\Omega) = i \sum_{j=0}^{n} \frac{b_\Omega(j)}{2[p_E b_E(j) + p_\Omega b_\Omega(j)]}. \tag{10}$$

We can estimate in the same way the phase space volume for a fixed value of y_0 by retracing the steps from Eqs. (6) to (9), but with the product and sums going from 1 to n instead of 0 to n. By combining these parametric representations, we obtain explicit expressions for the normalized PDFs of y_0 that are displayed as lines in Fig. 1(d) and are in good agreement with the numerical results [14].

Note that canonical distributions with quadratic invariants are Gaussian. When there is condensation of energy at large scale, only a few modes are present and then the canonical distribution has no reason to reproduce the microcanonical distribution results [15]. Indeed, $k_c^2 = \Omega/E < 5$ with $\Omega = (1^2 + 1^2)^2 y_0^2 + (1^2 + 2^2)^2 y_1^2 + \cdots$ and $E = (1^2 + 1^2) y_0^2 + (1^2 + 2^2) y_1^2 + \cdots$ implies that $y_0 \neq 0$. Thus the microcanonical PDF of y_0 has to obey $p(0) = 0$ for $k_c^2 < 5$ which forbids reversals of the large-scale circulation. This represents ergodicity breakdown. Our above results show that this breakdown is preceded by an ergodicity delay, in the sense that $p(0)$ becomes very small [16–18].

We now consider in more detail the regime with random reversals of the large-scale circulation and its transition to the condensed regime for which the flow no longer explores the whole phase space, keeping a given sign of the large-scale circulation. As shown above [compare Figs. 1(a) and 1(b)], the

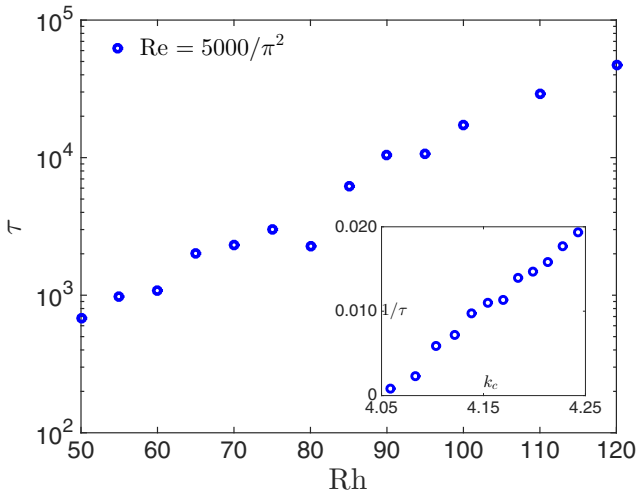

FIG. 2. Reversals: Log-linear plot of the mean waiting time τ between successive reversals versus Rh, obtained from our DNSs of NSE for $\mathrm{Re} = 5000/\pi^2$ (blue circles). Inset: Plot of the reversal frequency $1/\tau$ versus k_c from the DNSs of TEE; it shows that the reversal frequency decreases linearly with k_c with a critical $k_c^* \simeq 4.06$, below which the reversals are not observed for the integration time.

mean waiting time τ between successive reversals increases when Rh is increased in the NSE; respectively, k_c is decreased in the TEE. However, the divergence of τ does not follow the same law for the NSE and the TEE. Figure 2 shows an exponential increase of τ with Rh in the NSE, whereas a fit of the form $\tau \propto (k_c - k_c^*)^{-1}$ with $k_c^* \simeq 4.06$ is observed in the TEE (see inset of Fig. 2). The latter result is expected since there exists a critical value of k_c below which reversals are not possible in order to fulfill the conservation of both E and Ω. We thus expect that τ becomes infinite for a finite value of k_c. A similar trend is not observed in the NSE for τ versus Rh. This cannot be explained using the relation between k_c and Rh displayed in Fig. 1(c) that is roughly linear close to the transition to the condensed regime. In contrast to the TEE, the NSE does not involve conserved quantities that prevent reversals, even when Rh is large. In addition, all the modes above k_f that are suppressed in the TEE can act as an additional source of noise in the NSE and trigger reversals.

Although it can be expected that viscous dissipation is negligible for the dynamics of large scales, it is remarkable that taking into account the effect of large-scale friction by selecting the value of Ω/E in the initial conditions of the TEE is enough to describe the bifurcations of the large-scale flow using a small number of modes governed by the Euler equation. Thus, one discards the huge number of degrees of freedom related to small-scale turbulent fluctuations. In addition, equilibrium statistical mechanics, using the microcanonical distribution related to the TEE, correctly describes the PDF of the large-scale velocity in the different turbulent regimes. Transitions between different mean flows are widely observed in turbulent regimes, the most famous example being the drag crisis for which the wake of a sphere becomes narrower. Using the Navier-Stokes equation with noisy forcing [19] is a way to describe this type of transition. The TEE as presented here, can provide an alternative method to describe the dynamics of large scales in turbulence and to model a bifurcation of the mean flow on a strongly turbulent background.

We thank Francois Pétrélis for useful discussions. Support of the Indo-French Centre for the Promotion of Advanced Research (IFCPAR/CEFIPRA) Contract No. 4904-A is acknowledged. This work was granted access to the HPC resources of MesoPSL financed by the Region Ile de France and the project Equip@Meso (Reference No. ANR-10-EQPX-29-01) of the programme Investissements d'Avenir supervised by the Agence Nationale pour la Recherche. V.S. acknowledges support from EuHIT–European High-performance Infrastructure in Turbulence, which is funded by the European Commission Framework Program 7 (Grant No. 312778).

APPENDIX

We give here explicitly the set of 13 ODEs for the amplitudes of the Fourier modes $\hat{\psi}_{m,n}$ that define the TEE in the case $k_{\max} = 2\sqrt{5}$. Note that $\hat{\psi}_{m,n}$ are real numbers because of the free-slip boundary conditions (see text).

$$\frac{d\hat{\psi}_{11}}{dt} = \frac{1}{2}[(2\hat{\psi}_{12} + 5\hat{\psi}_{14})\hat{\psi}_{23} + \hat{\psi}_{13}(2\hat{\psi}_{22} + 5\hat{\psi}_{24}) - 2\hat{\psi}_{22}\hat{\psi}_{31} - \hat{\psi}_{32}(2\hat{\psi}_{21} + 5\hat{\psi}_{41}) + 3\hat{\psi}_{33}(\hat{\psi}_{24} - \hat{\psi}_{42}) - 5\hat{\psi}_{31}\hat{\psi}_{42}], \quad \text{(A1)}$$

$$\frac{d\hat{\psi}_{12}}{dt} = \frac{1}{20}[25\hat{\psi}_{13}\hat{\psi}_{21} + 54\hat{\psi}_{14}\hat{\psi}_{22} + \hat{\psi}_{11}(9\hat{\psi}_{21} - 11\hat{\psi}_{23}) + 25\hat{\psi}_{21}\hat{\psi}_{31} + 21\hat{\psi}_{23}\hat{\psi}_{31} + 56\hat{\psi}_{24}\hat{\psi}_{32} - 39\hat{\psi}_{21}\hat{\psi}_{33} + 49\hat{\psi}_{31}\hat{\psi}_{41} + 9\hat{\psi}_{33}\hat{\psi}_{41}], \quad \text{(A2)}$$

$$\frac{d\hat{\psi}_{21}}{dt} = \frac{1}{20}[-49\hat{\psi}_{13}\hat{\psi}_{14} - \hat{\psi}_{11}(9\hat{\psi}_{12} - 11\hat{\psi}_{32}) - 21\hat{\psi}_{13}\hat{\psi}_{32} - \hat{\psi}_{12}(25\hat{\psi}_{13} + 25\hat{\psi}_{31} - 39\hat{\psi}_{33}) - 9\hat{\psi}_{14}\hat{\psi}_{33} - 54\hat{\psi}_{22}\hat{\psi}_{41} - 56\hat{\psi}_{23}\hat{\psi}_{42}], \quad \text{(A3)}$$

$$\frac{d\hat{\psi}_{22}}{dt} = \frac{1}{4}[-9\hat{\psi}_{12}\hat{\psi}_{14} - 4\hat{\psi}_{11}(\hat{\psi}_{13} - \hat{\psi}_{31}) + 5\hat{\psi}_{14}\hat{\psi}_{32} + 9\hat{\psi}_{21}\hat{\psi}_{41} - 5\hat{\psi}_{23}\hat{\psi}_{41}], \quad \text{(A4)}$$

$$\frac{d\hat{\psi}_{13}}{dt} = \frac{1}{10}\{\hat{\psi}_{11}(6\hat{\psi}_{22} - 9\hat{\psi}_{24}) + 7\hat{\psi}_{21}(3\hat{\psi}_{14} + 2\hat{\psi}_{32}) + 11\hat{\psi}_{32}\hat{\psi}_{41} + \hat{\psi}_{31}[4\hat{\psi}_{22} + 25(\hat{\psi}_{24} + \hat{\psi}_{42})]\}, \quad \text{(A5)}$$

$$\frac{d\hat{\psi}_{31}}{dt} = \frac{1}{10}\{-14\hat{\psi}_{12}\hat{\psi}_{23} - 11\hat{\psi}_{14}\hat{\psi}_{23} - 21\hat{\psi}_{12}\hat{\psi}_{41} - \hat{\psi}_{11}(6\hat{\psi}_{22} - 9\hat{\psi}_{42}) - \hat{\psi}_{13}[4\hat{\psi}_{22} + 25(\hat{\psi}_{24} + \hat{\psi}_{42}]\}, \tag{A6}$$

$$\frac{d\hat{\psi}_{23}}{dt} = \frac{1}{52}[35\hat{\psi}_{12}\hat{\psi}_{31} + 77\hat{\psi}_{14}\hat{\psi}_{31} + \hat{\psi}_{11}(3\hat{\psi}_{12} - 75\hat{\psi}_{14} + 55\hat{\psi}_{32}) + 90\hat{\psi}_{22}\hat{\psi}_{41} + 42\hat{\psi}_{24}\hat{\psi}_{41} + 120\hat{\psi}_{21}\hat{\psi}_{42}], \tag{A7}$$

$$\frac{d\hat{\psi}_{32}}{dt} = \frac{1}{52}\{-\hat{\psi}_{11}(3\hat{\psi}_{21} + 55\hat{\psi}_{23} - 75\hat{\psi}_{41}) - 7\hat{\psi}_{13}(5\hat{\psi}_{21} + 11\hat{\psi}_{41}) - 6[20\hat{\psi}_{12}\hat{\psi}_{24} + \hat{\psi}_{14}(15\hat{\psi}_{22} + 7\hat{\psi}_{42})]\}, \tag{A8}$$

$$\frac{d\hat{\psi}_{14}}{dt} = \frac{1}{68}[-35\hat{\psi}_{13}\hat{\psi}_{21} + 18\hat{\psi}_{12}\hat{\psi}_{22} + 55\hat{\psi}_{11}\hat{\psi}_{23} - 33\hat{\psi}_{23}\hat{\psi}_{31} + 50\hat{\psi}_{22}\hat{\psi}_{32} + 117\hat{\psi}_{21}\hat{\psi}_{33} - 15\hat{\psi}_{33}\hat{\psi}_{41} + 98\hat{\psi}_{32}\hat{\psi}_{42}], \tag{A9}$$

$$\frac{d\hat{\psi}_{41}}{dt} = \frac{1}{68}[-18\hat{\psi}_{21}\hat{\psi}_{22} - 50\hat{\psi}_{22}\hat{\psi}_{23} - 98\hat{\psi}_{23}\hat{\psi}_{24} + 35\hat{\psi}_{12}\hat{\psi}_{31} - 55\hat{\psi}_{11}\hat{\psi}_{32} + 33\hat{\psi}_{13}\hat{\psi}_{32} - 117\hat{\psi}_{12}\hat{\psi}_{33} + 15\hat{\psi}_{14}\hat{\psi}_{33}], \tag{A10}$$

$$\frac{d\hat{\psi}_{24}}{dt} = \tfrac{1}{10}[8\hat{\psi}_{12}\hat{\psi}_{32} + 2\hat{\psi}_{11}(\hat{\psi}_{13} + 6\hat{\psi}_{33}) + 7\hat{\psi}_{23}\hat{\psi}_{41} + 18\hat{\psi}_{22}\hat{\psi}_{42}], \tag{A11}$$

$$\frac{d\hat{\psi}_{42}}{dt} = \frac{1}{10}[-8\hat{\psi}_{21}\hat{\psi}_{23} - 18\hat{\psi}_{22}\hat{\psi}_{24} - 2\hat{\psi}_{11}\hat{\psi}_{31} - 7\hat{\psi}_{14}\hat{\psi}_{32} - 12\hat{\psi}_{11}\hat{\psi}_{33}], \tag{A12}$$

$$\frac{d\hat{\psi}_{33}}{dt} = -\frac{3}{2}[\hat{\psi}_{14}\hat{\psi}_{21} - \hat{\psi}_{12}\hat{\psi}_{41} + \hat{\psi}_{11}(\hat{\psi}_{24} - \hat{\psi}_{42})]. \tag{A13}$$

The dynamical evolution of the above set of ODEs conserves the total energy and enstrophy, which are given by

$$E = (1^2+1^2)\hat{\psi}_{11}^2 + (1^2+2^2)\hat{\psi}_{12}^2 + (2^2+1^2)\hat{\psi}_{21}^2 + (2^2+2^2)\hat{\psi}_{22}^2 + (3^2+1^2)\hat{\psi}_{31}^2 + (1^2+3^2)\hat{\psi}_{13}^2 + (2^2+3^2)\hat{\psi}_{23}^2 + (3^2+2^2)\hat{\psi}_{32}^2 + (1^2+4^2)\hat{\psi}_{14}^2 + (4^2+1^2)\hat{\psi}_{41}^2 + (2^2+4^2)\hat{\psi}_{24}^2 + (4^2+2^2)\hat{\psi}_{42}^2 + (3^2+3^2)\hat{\psi}_{33}^2 \tag{A14}$$

and

$$\Omega = (1^2+1^2)^2\hat{\psi}_{11}^2 + (1^2+2^2)^2\hat{\psi}_{12}^2 + (2^2+1^2)^2\hat{\psi}_{21}^2 + (2^2+2^2)^2\hat{\psi}_{22}^2 + (3^2+1^2)^2\hat{\psi}_{31}^2 + (1^2+3^2)^2\hat{\psi}_{13}^2 + (2^2+3^2)^2\hat{\psi}_{23}^2 + (3^2+2^2)^2\hat{\psi}_{32}^2 + (1^2+4^2)^2\hat{\psi}_{14}^2 + (4^2+1^2)^2\hat{\psi}_{41}^2 + (2^2+4^2)^2\hat{\psi}_{24}^2 + (4^2+2^2)^2\hat{\psi}_{42}^2 + (3^2+3^2)^2\hat{\psi}_{33}^2. \tag{A15}$$

[1] R. H. Kraichnan, Phys. Fluids **10**, 1417 (1967).
[2] J. Sommeria, J. Fluid Mech. **170**, 139 (1986).
[3] J. Herault, F. Pétrélis, and S. Fauve, Europhys. Lett. **111**, 44002 (2015).
[4] P. K. Mishra, J. Herault, S. Fauve, and M. K. Verma, Phys. Rev. E **91**, 053005 (2015).
[5] D. Gottlieb and S. A. Orszag, *Numerical Analysis of Spectral Methods* (SIAM, Philadelphia, 1977).
[6] S. M. Cox and P. C. Matthews, J. Comput. Phys. **176**, 430 (2002).
[7] In the range of Rh studied here, $\hat{\psi}_{1,1}(t)$ makes the dominant contribution to three related quantities: (a) the large-scale circulation around the domain boundaries $\Gamma = \Sigma' 4(n^2 + m^2)\hat{\psi}_{nm}/nm$, where Σ' denotes the sum over jointly odd n,m; (b) $\psi(\pi/2,\pi/2) = \Sigma'\hat{\psi}_{nm}$, a quantity measured in Refs. [2,3] that represents the flow rate between the center of the container and its boundary, and (c) the fluid total angular momentum $L = 8\Sigma'\hat{\psi}_{nm}/nm$.
[8] R. H. Kraichnan, J. Fluid Mech. **67**, 155 (1975).
[9] T. D. Lee, Quart. Appl. Math. **10**, 69 (1952).
[10] Spectral truncation breaks the large-scale circulation conservation of the (untruncated) Euler equation. Note that this technical point is crucially needed for the TEE to be able to reproduce NSE reversals.
[11] J. Zinn-Justin, *Phase Transitions and Renormalization Group* (Oxford University Press, New York, 2007).
[12] C. M. Bender and S. A. Orszag, *Advanced Mathematical Methods for Scientists and Engineers*, International Series in Pure and Applied Mathematics (McGraw-Hill, Auckland, 1978).
[13] Purely imaginary values for (p_E, p_Ω) parametrize real values of (E,Ω).
[14] We have checked (data not shown) that the steepest-descent estimates correctly represent microcanonical Monte Carlo results, even in the highly bimodal regime.
[15] L. C. Kells and S. A. Orszag, Phys. Fluids **21**, 162 (1978).
[16] P. Dmitruk, P. D. Mininni, A. Pouquet, S. Servidio, and W. H. Matthaeus, Phys. Rev. E **90**, 043010 (2014).
[17] P. Dmitruk, P. D. Mininni, A. Pouquet, S. Servidio, and W. H. Matthaeus, Phys. Rev. E **83**, 066318 (2011).
[18] J. V. Shebalin, Phys. Lett. A **250**, 319 (1998).
[19] F. Bouchet and E. Simonnet, Phys. Rev. Lett. **102**, 094504 (2009).